ДГКМ
ДРУШТВО НА ГРАДЕЖНИТЕ КОНСТРУКТОРИ НА МАКЕДОНИЈА

Партизански одреди 24,
П.Фах 560, 1001 Скопје
Македонија

MASE
MACEDONIAN ASSOCIATION OF STRUCTURAL ENGINEERS

Partizanski odredi 24,
P. Box 560, 1001 Skopje
Macedonia

mase@gf.ukim.edu.mk
http://mase.gf.ukim.edu.mk

FE - 9

Јасмин ТКОЧ[1], Питер ХИК[2], Катерина ТИЕЛЕ[3], Герард ФИТ[4], Марија ДОЦЕВСКА[5], Питер МАРК[6]

ИСПИТУВАЊЕ И НУМЕРИЧКА СИМУЛАЦИЈА НА МИКРОАРМИРАНИ ПЛОЧИ ИЗЛОЖЕНИ НА ДЕЈСТВО НА ПОЖАР

РЕЗИМЕ

Однесувањето на микроармиран бетон изложен на дејство на пожар е анализирано експериментално. Направени се испитувања на микроармирани плочи со и без дополнителна конвенционална арматура истовремено изложени на едностране пожарно сценарио и механичко оптоварување. Поточно, во експериментот испитуван е преносот на топлината на бетон со различно количество на челични влакна, како и неговите температурно зависни деформации. Врз основа на обработените резултати, подготвени се дијаграми за димензионирање кои овозможуваат директно определување на капацитетот на носивост на свиткување на микроармирани попречни пресеци со дополнителна арматура изложени на влијание на температура според временско-температурната рамномерна крива за 90 минути.

Клучни зборови: микроармиран бетон, пожар, пренос на топлина, капацитет на носивост

Jasmin TKOCZ[1], Peter HEEK[2], Catherina THIELE[3], Gerhard VITT[4], Marija DOCEVSKA[5], Peter MARK[6]

TESTS AND NUMERICAL SIMULATION OF SFRC SLABS EXPOSED TO FIRE

SUMMARY

The behaviour of steel fibre reinforced concrete (SFRC) exposed to fire is experimentally analysed. Tests on SFRC slabs with and without rebars subjected to one-sided elevated temperature and mechanical loading are performed. In detail, the heat transmission of concrete containing variable dosages of steel fibres and its temperature-dependent load-deformation behaviour is investigated in experiments. Results are processed and a design chart is prepared to allow for an assessment of load bearing capacities of SFRC cross-sections with rebars subjected to temperature impact according to a uniform-temperature-time-curve (UTTC) for 90 minutes (R90).

Keywords: Steel fibre reinforced concrete, fire, heat transmission, bearing capacity, design chart

The present paper is extracted from ALITinform International Analytical Review 41(6), 2015, pages 36–53 (Tkocz et al. 2015).

[1] M. Sc., jasmin.tkocz@rub.de
[2] M. Sc., peter.heek@rub.de
[3] Jun.-Prof. Dr.-Ing., Department of Civil Engineering, Technical University Kaiserslautern, Kaiserslautern, Germany, catherina.thiele@bauing.uni-kl.de
[4] Dipl.-Ing., Bekaert GmbH, Neu-Anspach, Germany, gerhard.vitt@bekaert.com
[5] M. Sc., Faculty of Civil Engineering, University "Ss. Cyril and Methodius", Skopje, Republic of Macedonia, docevska.marija@yahoo.com
[6] Prof. Dr.-Ing. habil., peter.mark@rub.de
[1], [2], [6], Faculty of Civil and Environmental Engineering, Ruhr-University Bochum, Bochum, Germany

1. INTRODUCTION

The present paper is based on a cooperation between two German universities, namely the Technical University of Kaiserslautern and the Ruhr-University of Bochum. It is motivated by recently updated design codes for steel fibre reinforced concrete (SFRC), more precisely by its regulations concerning SFRC structures exposed to fire. The fundamental benefit of combining conventional reinforcement with additional steel fibres is the transfer of tensile forces after cracking of the concrete. Then steel fibres bridge cracks brace-like and significantly reduce crack widths and spacing. This generally leads to higher bearing capacities in bending or shear and consequently lowers the required amount of conventional steel reinforcement in structural design (DAfStb 2015 b).

However, in case of a fire resistant design, a reduction of reinforcement due to additional steel fibres is not covered by current standards. In fact, the temperature- and crack width-dependent behaviour of the post-cracking tensile strength in SFRC structures is subject of ongoing research. In this context, the impact on the heat transmission within the structure is controversially discussed. On the one hand additional steel appears to accelerate the heating rate (Diederichs 1999), on the other hand it is argued that steel fibres prevent concrete from spalling and thus protect the inner structure from direct exposure to fire (Hertel et al. 2002). To check the significance of these intensively discussed statements by means of full-scale tests, six SFRC concrete plates are subjected to elevated temperatures due to the uniform-temperature-time-curve (UTTC) and mechanical loading in experiments.

Three types of general design requirements to be met are stated in DIN EN 1992-1-2: resistance (R), integrity (E) and insulation (I). Since the latter two are out of the focus of this contribution the fire resistance (R) of the specimens can be ensured holding on standardized design solutions in terms of tabular data or simplified or general design procedures. This is admissible since the objective of these fire tests is solely the investigation of the heat transfer within SFRC and the temperature-dependent development of the post-cracking strength.

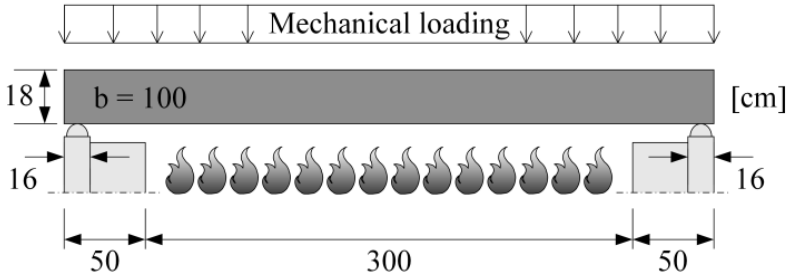

Fig. 1. Test setup.

No.:	Reinforcing mat	Steel fibre dosage [kg/m³]	L1/L2 [MN/m²]/[MN/m²]	$M_{Rd,\theta=20°C}$ [kNm]	Fibre bearing ratio [%]	UTTC
P1	R335 *	-	-	23.6	0	yes
P2	R335 *	40	2.7/2.1	41.1	42.2	yes
P3	R188 **	40	2.7/2.1	30.7	54.4	yes
P4	R188 **	80	3.0/3.0	37.6	62.7	yes
P5	-	40	1.8/1.2	11.1	100	no
P6	-	40	1.8/1.2	11.1	100	yes
P7	-	80	3.0/2.7	20.3	100	no
P8	-	80	3.0/2.7	20.3	100	yes
* prov. reinforcement 3,35 cm²/m lengthwise, ~ 20 % across ** prov. reinforcement 1,88 cm²/m lengthwise, ~ 20 % across						

Table 1. General properties and design resistances of specimens.

2. FIRE TESTS ON CONCRETE SLABS

The test matrix in Table 1 comprises properties and calculative design resistances of the six concrete specimens reinforced with different amounts of steel fibres and conventional reinforcing mats. Additionally, two load bearing tests under normal temperature conditions are conducted on true replicates (P5 & P7) of the purely fibre reinforced specimens P6 and P8. Besides, the uniform size of all the test specimens, sketched in Fig. 1, represents typical dimensions for reinforced concrete ceiling plates (l x w x h = 400 x 100 x 18 cm).

A fundamental design objective has been to align – as good as possible – the load bearing capacities of all specimens under normal temperature ($M_{Rd,\vartheta=20°C}$). The tensile forces induced by bending are born proportionally by the mesh and the steel fibre reinforcement that is chosen to various amount combinations within the specimens. The fibre bearing ratio quantifies the fibre's contribution to the total resistance. Accompanying four-point bending tests according to the guideline "Steel Fibre Reinforced Concrete" (DAfStb 2015 b) of the German Committee for Reinforced Concrete (DAfStb) on slabs of the corresponding mixture deliver information on the factually attained values after concreting. Due to a strong scatter in the post-cracking tensile strength of SFRC (DAfStb 2015 a), the objective of comparable results is only achieved in an approximate way for the specimens P1 to P4. Based on the bending tests the specimen's performance class (denoted by L) according to (DAfStb 2015 b) can be derived. L1 and L2 describe the characteristic values of residual flexural strengths after cracking at 0.5 or 3.5 mm deflection.

The concrete composition (C35/45) purposely contains a great amount of cement paste and fines that ensure a very soft consistency to be commonly adapted for high steel fibre dosages. Thereby, the size distribution of the quartzitic aggregates is continuous with a maximum grain size of 16 mm. In construction practice a volume fraction of fibre reinforcement between 0.25 and 1 % is typical, whereas 40 kg/m^3 corresponds to a volume fraction of 0.5 %. The hooked-end macro fibres of type Dramix 5D 65/60BG or Dramix 3D 65/60BG of NV Bekaert SA are added to the concrete by a compulsory mixer to ensure a homogeneous dispersal. After concreting, the test specimens have to be conditioned for at least three months (DAfStb 2015 a). Additionally, they have been dried actively to get a moisture content comparable to practice-relevant structures and to avoid unintended concrete spalling by a water induced gas pressure during fire exposition. As required from (DAfStb 2015 a) the moisture referenced to ground at testing time lies always between 1 and 5 %.

2.1. Load, measuring device and performance

In the fire tests the specimens are subjected to both thermal and mechanical loading. The mechanical load is realized by stacked-on metal sheets, while a furnace delivers the thermal load. An enclosed fire room is created exposing the plate on the exterior walls of the furnace and providing insulation elsewhere. Gas powered burners perform the standardized logarithmic temperature trend of the UTTC, internationally known as ISO-curve. Consequently, one-sided thermal loading is induced. Due to the two half shells serving as line supports, the effective length of the specimens amounts to l_{eff} = 384 cm, whereas only the inner part (l_{UTTC} = 300 cm) is exposed to the fire directly. Hence, the effective temperature exposed length is chosen to the average of both lengths, namely $l_{eff,UTTC} \approx$ 342 cm. This initial assumption could be confirmed by thermographic images taken during the cooling phase that revealed a matching temperature distribution in longitudinal direction. Transversely the total width was evenly heated.

With regard to the two different load impacts, the measuring equipment comprises inductive sensors to record vertical displacements at the quarter points of the effective length and sensors to register the temperature at certain intervals during the fire tests. Up to in total 26 measurement points are placed along a grid of five measuring axes length- and three axes crosswise, either on bottom and top sides, or distributed over the section height. Additionally, panel thermometers are installed to control the temperature within the furnace. For economic reasons, especially the enormous costs of the burner's fuel, the duration of the fire tests has been limited to 120 minutes.

For ultimate limit state, a maximum mid-span deflection and rate of deflections per second apply as stated in (DAfStb 2015 a). The time a structure withstands thermal exposition without exceeding these

limits, is defined by the fire resistance duration declared in minutes. For common structural elements a fire resistance of 90 minutes (R90) is usually claimed for in design.

2.2. Test results

Since specimens P5 and P7 were tested in normal temperature conditions solely and measuring devices failed while testing P2, five results remain to be interpreted. Both SFRC slabs without rebar (P6 & P8) failed prematurely as expected (7 min & 41 min ≤ 90 min) at mid-span showing one single crack due to the statically determinate test-setup. Unlike the remaining ones (P1, P3 and P4) which all show similar crack patterns characterized by regularly distributed and fine cracks along with large deflections.

As expected the furnace heating curve (UTTC) in Fig. 2.a generally runs ahead but affine to the temperature-dependent total deflections δ_{tot} of the specimens P1, P3 and P4 at mid-span. From thermography analysis a nonlinear temperature profile over the cross-section height can be reported having its maximum on the fire facing side and its minimum on the opposite face, while the temperature distribution in longitudinal and transversal direction remains uniform everywhere but close to the supports.

Comparing the experimental curves among themselves it becomes obvious that the displacements of the bar reinforced specimen P1 always exceed the ones of P3 and P4 with additional fibre contents of 40 kg/m^3 and 80 kg/m^3. However, the deflection curves assimilate with time of temperature-exposition and increasing fire induced stresses as shown in Fig. 2.b. Here, the total deflections of P3 and P4 were measured and related to the ones of P1 at three different locations and five temperature instants. Linear trend lines confirm convergence. Simultaneously, the scatter of the total mid-span deflections by means of its coefficient of variation V_δ decreases.

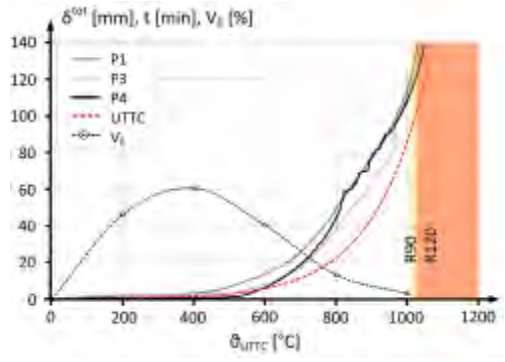

Fig. 2.a Temperature-deflection curves at mid-span of P1, P3 and P4.

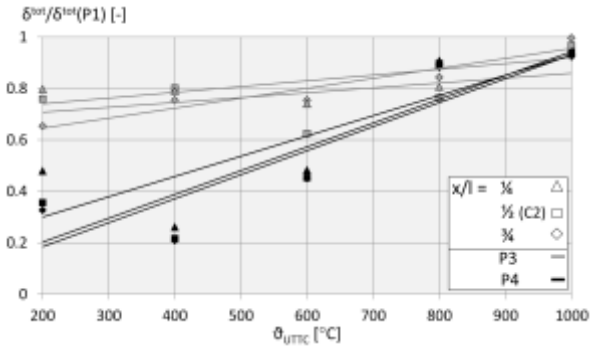

Fig. 2.b Temperature-dependent deflections of P3 and P4 related to P1.

3. ANALYSIS

The following analysis of test data is split into heat transfer mechanisms and temperature-dependent load-deformation behaviour. Experimental results serve to verify calculative models in both cases.

3.1. Heat transmission model

To determine the temperature profile over the cross-section's height of a heated specimen, a numerical spreadsheet model that idealises the cross-section and its boundaries by a set of perpendicular cells (denoted elements), is developed in Microsoft Excel®.

Starting from the first law of thermodynamics, the differential equation of heat-flux by Fourier can be deduced (Mannsfeld 2011). Accordingly, the flux in solids depends on the materials involved, their temperature-dependent properties and the nonlinear temperature loading itself (UTTC). Here, the temperature profile is calculated incrementally employing a scheme sketched in Fig. 3. Depending on an initially defined ambient temperature field (ϑ_{t0} = 20 °C), the temperature load due to UTTC on bottom side is calculated and updated per time increment and cell of the cross-section. Hence, each cell must be attributed either to an element made from concrete, rebar or SFRC, accounting for specific temperature-

dependent properties, or a boundary element getting indicators to mark environmental conditions (e.g. fire-exposed or not). While in the thermal exchange between two adjacent solid elements the principle of conduction applies with boundary elements convection and radiation have to be taken into account.

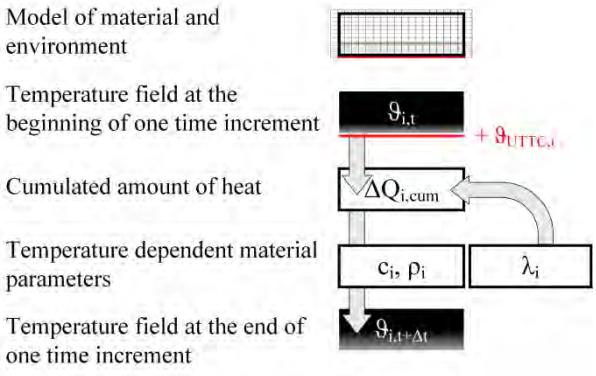

Fig. 3. Concept of the heat transmission model.

Employing Eq. (1), specific temperature-dependent material parameters of concrete (DIN 2010 a) and steel (DIN 2010 b), e.g. density ρ, heat capacity c_p, conductivity λ, are combined to form a virtually set of smeared material parameters for SFRC with variable amounts of fibres. Its computation considers the individual volume fractions in every element. The same is applied to account for section layers containing mesh reinforcement.

$$P_{sc} = a_s \cdot P_s + a_c \cdot P_c \quad (1)$$

with
P_{sc} Smeared parameter
P_s Parameter of steel
P_c Parameter of concrete
a_s Relative amount of steel [%]
a_c Relative amount of concrete [%]

3.1.1. Results

The heat transmission model provides the cross-section's temperature profile for a pre-defined duration of fire exposition in every time step. Fig. 4 exemplifies such results obtained from a homogeneous concrete section under thermal load according to UTTC from the bottom. It serves as reference for comparison with temperature profiles calculated with smeared thermal parameters.

Prior to the experimental fire tests, the heat transfer behaviour in SFRC cross-sections with respect to fire duration and cross-sectional height is investigated, based on the theoretical model. Steel fibre volume fractions between 0 and 2 % that are commonly used in construction practice are considered. From this study it is learned that the temperature increases theoretically with higher amounts of steel fibres. Generally, the increase lasts the longer the fire burns, whereas the trend decreases with less distance to the fire-treated side.

The modeling of rebar, i.e. 3D concrete-embedded reinforcement meshes, by 2D elements based on the principle of smeared parameters (c.f. Section 3.1) affects the temperature calculation significantly due to an erratic increase in the temperature curve and theoretically leads to higher temperatures on the slab's surface in general. Besides, the implementation of steel reinforcement layers is subject of controversial discussion among experts. Some claim to disregard small bar diameters in heat transmission models due to the restriction on a small layer (vfdb 2013).

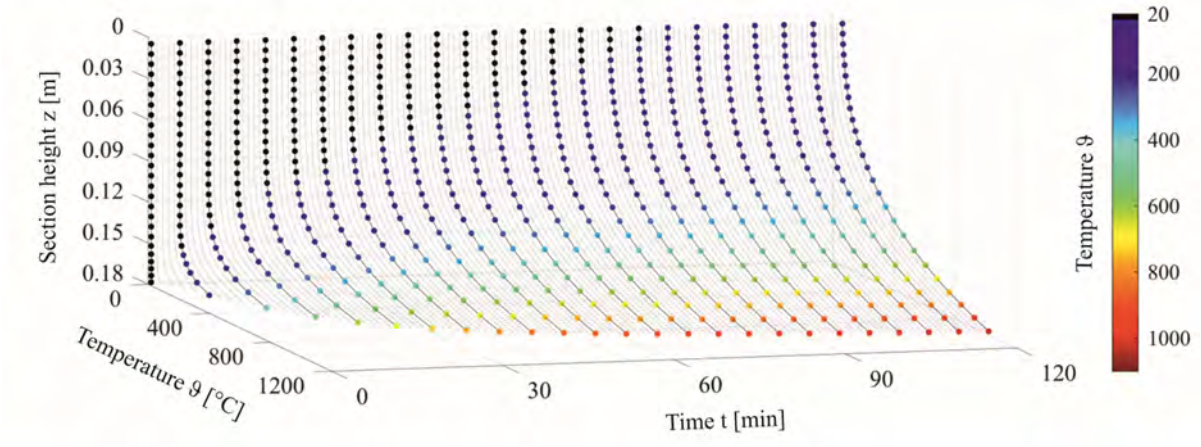

Fig. 4. Reference simulation of plain concrete – time-dependent temperature profile of the cross-section.

3.1.2. Verification

The experimental temperature data obtained from testing of specimens P1, P3 and P4 are compared to the numerically computed ones in Fig. 5. On the left, the absolute temperature profiles over the cross-section height for the three fibre amounts investigated (0, 0.5 and 1.0 vol.-% referring to P1, P3 and P4) are illustrated to three time instants (t_i = 15, 60 and 120 minutes). Dashed lines represent calculated temperatures, predicted by the heat transmission model disregarding reinforcement mats, while checkmarks are attributed to experimental test data. On the right, the same but relative data are shown in a matrix form. Every cell contains an individual data set with respect to fibre amount and time of fire exposition. It can be seen that the related measurement data predominantly lay below the dividing line. Thus, the calculation model tends to overestimate the temperature. However, with regard to forecasting and verification, calculated fire resistances based on temperature contour lines, are conservative.

In comparison and since the scatter in the experimental thermal data is generally large, the marginal theoretical acceleration of heat transmission caused by higher steel fibre amounts might be neglected. The calculated and experimental results are in general accordance, if thermal material parameters of plain concrete are also used for SFRC as recommended in (DBV 2001).

Furthermore, explicit modeling of rebar can obviously be neglected in numerical calculations of heat transfer within concrete structures. The effect of an erratic increase observed in Section 3.1.1 due to implementation of reinforcement layers cannot be confirmed by the experimental temperature data obtained here. In fact, the calculation neglecting explicit steel reinforcement delivered results closer to actually measured data. Therefore, further simulations are carried out without taking into account local bar or mesh reinforcements. The cross-section is assumed to be homogeneous, wherein the steel contents or rather the corresponding steel fibre amount, is smeared by adjusted thermal material parameters.

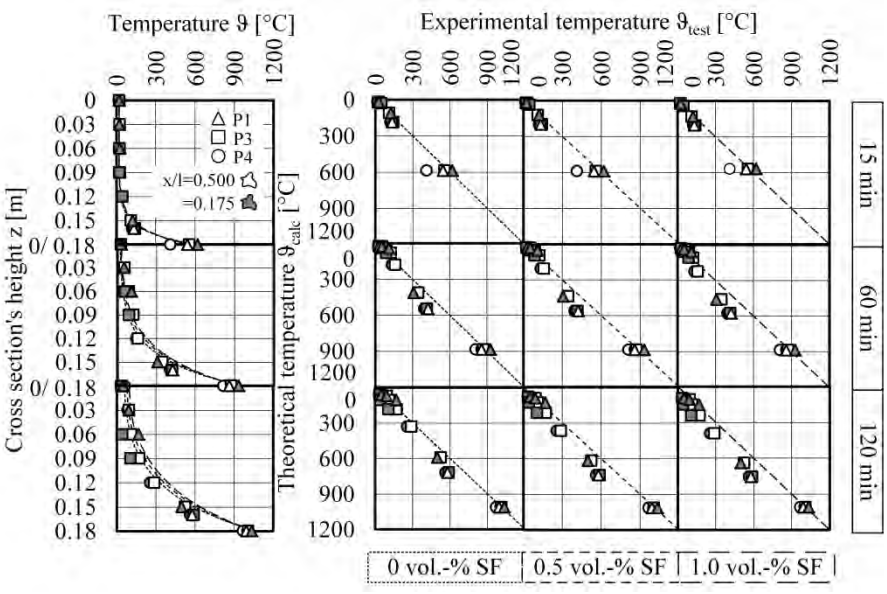

Fig. 5. Experimental versus calculated results by means of absolute and relative temperatures of a concrete cross-section containing fibre amounts of 0, 0.5 and 1.0 vol.-% subjected to one-sided fire for 15, 60 and 120 minutes.

Next, the sensitivity of the results with respect to the most important parameters involved shall be discussed. These are: the number of elements in discretization, the size of the time step, the moisture of the specimen, the heat transfer coefficients, the consideration of steel reinforcement and the thermal conductivity of concrete. Information on the latter one is directly contained in current standards like EC 2. Here a range of variation between an upper and lower limit of temperature-dependent thermal conductivity is defined. However, parametric studies lead to more realistic values using the lower limit (DIN 2010 a). A fact also accounted for by EC 2, where contour lines based on the lower limit of the thermal conductivity of concrete are provided in its appendix A.

3.2. Determination of deformations

As long as multiple cracking occurs, the temperature-dependent load bearing capacity of concrete girders might be analysed regarding their deflections by moment-curvature relations. Generally, deflections integrate the load- and stiffness-dependent material behaviour of concrete. Usually, the course of deflections along a girder's length is obtained from integration of the curvature (κ) times a virtual moment from unit deformation $\bar{M}$ at all points of interest (c.f. Eq. 5). Reminding Bernoulli's hypothesis, the curvature is well-defined with respect to two strains: the concrete strain at the outermost fibre of a cross-section in compression (ε_{c2}) and the strain at the position of rebar (ε_{s1}). Its load-dependency with respect to combinations of bending moments and axial forces is expediently covered by means of a moment curvature-relationship reflecting all possible states of equilibrium on cross-sectional level. From Eq. (2) and according to (DIN 2010 a) the total curvature might be additively split into thermal (superscript "th") and mechanical induced (superscript "σ") portions. Therein, M denotes the bending moment and EI the related stiffness while d is the distance from the rebar to the outer compressive fibre of the section.

$$\kappa = \kappa^{\sigma} + \kappa^{th} = \frac{M}{EI} = \frac{\left|\varepsilon_{c2}^{ges}\right| + \varepsilon_{sl}^{ges}}{d} = \frac{\left(\left|\varepsilon_{c2}^{\sigma}\right| + \left|\varepsilon_{c2}^{th}\right|\right) + \left(\varepsilon_{sl}^{\sigma} + \varepsilon_{sl}^{th}\right)}{d} \tag{2}$$

Consequently, the first step in the numerical recalculation of experimental data (specimens P1, P3, P4) must be a separation of temperature- and stress-dependent deformations due to fire and mechanical loading.

3.2.1. Thermal induced deformations

An arbitrary temperature profile of a cross-section can be dissembled into constant, linear and nonlinear portions as illustrated in Fig. 6.

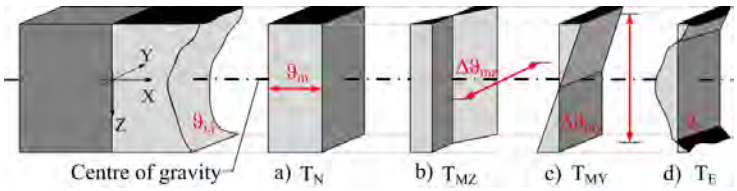

Fig. 6. Split of a temperature profile in constant, linear and nonlinear portions w.r.t. (Zichner 1976).

The mean temperature ϑ_m is obtained from the temperature data ϑ integrated over the total cross-section and divided by its area A. Thus, for a regularly discretized cross-section ϑ_m reads:

$$\vartheta_m \cong \frac{1}{A}\sum_i\sum_j \vartheta_{i,j} A_{i,j} \ , \tag{3}$$

wherein i and j denote cell indices of the regular grid chosen that subdivides the section into fibres. Furthermore, the linear temperature gradient $\Delta\vartheta$ about the y-axis in Fig. 6 can be estimated to:

$$\Delta\vartheta \cong \frac{h}{I_y}\sum_i\sum_j \vartheta_{i,j} z_{i,j} A_{i,j} \ , \tag{4}$$

wherein h denotes the cross-section height, I_y the moment of inertia about the y-axis and $z_{i,j}$ the distance of a fibre's center of gravity to the section's one. Since no linear temperature gradients about other axes exist in our case (one-sided heating), the residual is completely attributed to the nonlinear contribution.

For a global but simplified analysis of deflections it is sufficient to account for the linear temperature gradient only and neglect constant as well as nonlinear contributions. Taking these assumptions, thermal induced deformations can be derived based on the principle of virtual work by integration of the temperature induced curvature times a virtual moment from unit deformation at all points of interest along the girder's length considering the effective cross-section area exposed to fire (342 x 100 cm) only.

$$\delta^{th}(x) = \int_o^l \overline{M}(x) \cdot \kappa^{th}(\vartheta) \cdot dx = \int_o^l \overline{M}(x) \frac{\alpha_T(\vartheta) \cdot \Delta\vartheta}{h} dx \tag{5}$$

Due to simplification the thermal curvature $\kappa^{th}(\vartheta)$ in Eq. (5) is a function of the linear temperature gradient $\Delta\vartheta$, the coefficient of thermal expansion $\alpha_T(\vartheta)$ and the thermal concrete strains ε_{th} acc. to (DIN 2010 a).

Since neither heat transmission tests nor experimentally obtained load deformation curves have shown evidence to distinguish specimens with steel fibres (P3, P4) from others (P1) without when temperature rises, thermal strains ε_{th} of plain concretes and concretes containing common steel fibre amounts are considered equal.

3.2.2. Temperature-modified material behaviour

Mechanical loading of specimens causes initial deformations that increase with rising temperature due to softening material behaviour. EC 2 provides stress-strain relations of rebar and concrete in compression directly, by means of a reduced stiffness with higher temperature defining dimensionless reduction factors (DIN 2010 a). But, the temperature- and crack-width-dependent behaviour of SFRC is not yet defined in standards. It is rather object of vital research.

E.g. test results gained on recycled aggregate concrete containing amounts of steel fibres up to 1.5 vol.-% indicate enhanced temperature-dependent compressive strengths, moduli of elasticity as well as

energy absorption capacities compared to plain concrete (Chen et al. 2014). In (Falkner and Grunert 2011, Khaliq and Kodur 2011) reduced concrete spalling in case of SFRC exposed to fire due to an increased residual tensile strength is reported on. (Khaliq and Kodur 2011) limits a beneficial influence of steel fibres on spalling to a certain extent, because of a progressive loss of strength and bond of single fibres. Other experimental data published in (Balazs and Lubloy 2012, Holschemacher and Weiße 2004) shows that bond between rebar and SFRC is not significantly influenced by steel fibres in cases of both fire and normal temperatures. The authors in (Colombo 2006, Caverzan 2010) conclude, based on tensile and flexural tensile tests of SFRC subjected to elevated temperatures that the crack-width-dependent post cracking flexural tensile strength of SFRC acts similar to the flexural tensile strength in fire. On the other hand, the same tests indicate reduced softening of post cracking tensile strength compared to tensile strength in fire. Double-punch tests (Kim et al. 2015) conducted on different SFRCs confirm these observations but additionally point out a large scatter of the post cracking tensile strength with rising temperature and crack tip opening displacement (CTOD).

Fig. 7 sketches the experimental data collected from various literature sources as well as closed formulas suggested so far for plain concrete in tension (e.g. (DIN 2010 a)) and SFRC (DBV 2001). All formulas obviously define a relatively reduced tensile strength of concrete in case of elevated temperatures, more or less supported by the experiments.

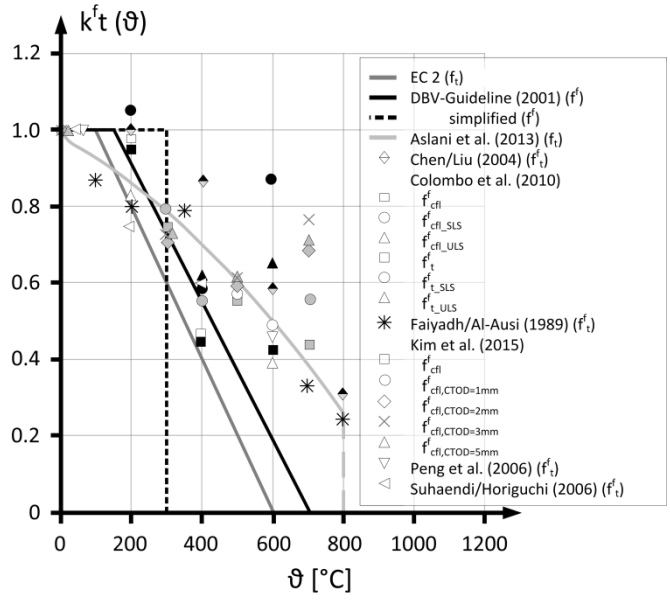

Fig. 7. Relative temperature- and crack-width-dependent softening of the post-cracking tensile strength of concrete (f_t) and SFRC (f^f_t).

Hence in the remainder, the temperature-dependent softening of both tensile and post cracking tensile strengths of SFRC is modelled acc. to Eq. (6) from (DBV 2001). It is represented by the full black lines in Fig. 7. The approach is independent from crack widths and strains but accounts for the temperature. On average it gathers the global trend in the data rather conservatively.

$$k^f_t(\vartheta) = \begin{cases} 1.0 & 20 \leq \vartheta < 150\ °C \\ 1.0 - 1.0 \cdot (\vartheta - 150\ °C) / 550\ °C & 150 \leq \vartheta \leq 700\ °C \\ 0 & > 700\ °C \end{cases} \quad (6)$$

with $k^f_t(\vartheta) = f^f(\vartheta = 20\ °C) / f^f(\vartheta)$

3.2.2. Mechanical induced deformations

For both, namely to recalculate experimental load deformation curves of the specimens P1, P3 and P4 and to derive design charts, additional specifications are necessary. A calculative but artificial modulus

of elasticity of concrete in compression acc. to EC 2 is adopted for tension as well, integrating elastic as well as plastic strains and high-temperature-creeping (Hosser et al. 2013). The post cracking tensile strength is modelled via multilinear stress-strain curves according to (DAfStb 2015 b). For simplification, tension stiffening is neglected due to generally reduced tension stiffening bond factors in case of SFRC (Heek and Mark 2014). All these parameters and the temperature-dependent stress-strain curves of quarzitic aggregate concrete and cold-formed rebar provided by EC 2 are implemented in a lamella model of the specimens. Technically, the cross-sectional height is subdivided into a finite number of layers, each having a constant temperature- and load-dependent stress-state of concrete in every time-instant. Then, with respect to provided reinforcement amounts and a fixed mechanical load, equilibrium is found, iteratively varying the strains. Generally, optimisation methods are suited to compute valid equilibrium states (Mark 2003). The governing equations can be derived from the familiar equilibrium conditions acc. to Eq. (7) and (8):

$$\Sigma N = 0 = \iint_{A_c} \sigma_c(\vartheta) dA_c + \iint_{A_c} \sigma_t(\vartheta) dA_c + A_{sl} \cdot \sigma_{sl}(\vartheta) \tag{7}$$

$$\Sigma M = 0 = \iint_{A_c} \sigma_c(\vartheta) \cdot z_c \cdot dA_c + \iint_{A_c} \sigma_t(\vartheta) \cdot z_c \cdot dA_c + + A_{sl} \cdot \sigma_{sl}(\vartheta) \cdot d_l - M_{Ed} \tag{8}$$

Results are moments and the corresponding strain states, like it is exemplarily shown in Fig. 8. From these, a moment-curvature relation can be established. Of course, for each cross-section considered, an individual moment-curvature relation must be derived either using design or mean material parameters.

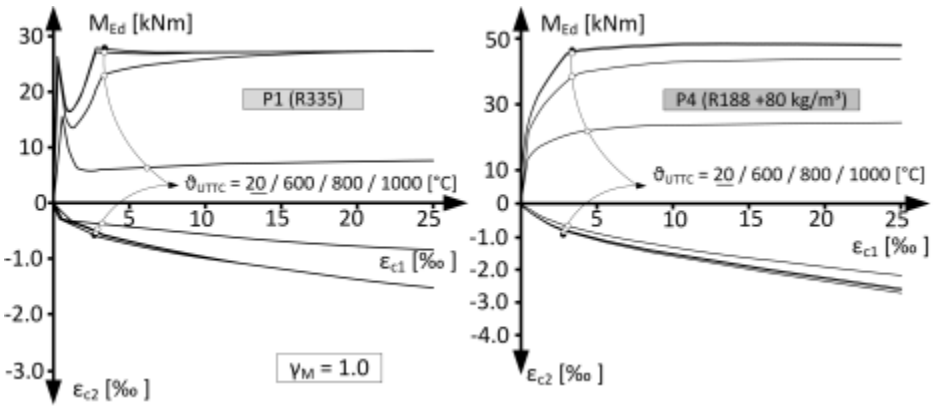

Fig. 8. Temperature-dependent relation of bending moment and concrete strains in case of P1 and P4.

Generally, Fig. 8 highlights that steel fibres can provide benefits in terms of temperature-dependent load bearing capacities and the load deformation behaviour itself contrasting SFRC with rebar to reinforced concrete. On the left, results of the purely bar-reinforced specimen P1 are shown, while P4 on the right contains additional steel fibres. The solid curve marked with a black dot represents results at a temperature of 20 °C. Tracing other solid curves marked with unfilled dots representing higher temperatures, it becomes obvious that with rising temperature the bending resistance decreases meanwhile deformations increase. In both cases, material softening starts with temperatures above ϑ_{UTTK} > 600 °C but the relative differences between two consecutive temperatures is smaller in case of additional fibres (specimen P4). This mainly results from the reinforcement's position close to the specimen's edge subjected to elevated temperatures while fibres are randomly spread over the whole tensile zone. Hence, not all fibres are similarly exposed to elevated temperatures due to one-sided heating and a strongly nonlinear shape of the temperature profile over the cross-section's height (c.f. Fig. 4).

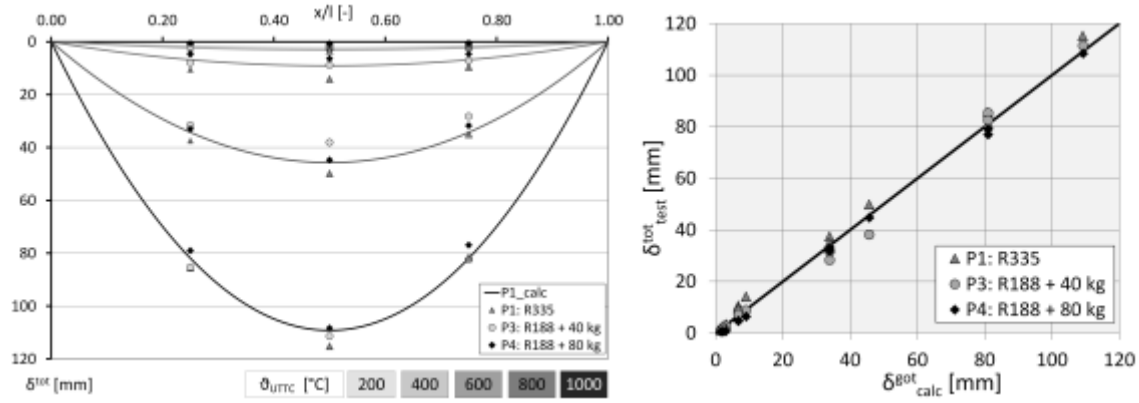

Fig. 9. Measured and calculated deflections of specimens P1, P3 and P4.

Finally, the moment-curvature-relationships obtained before are employed to recalculate the experimental deformation data to certain time instants acc. to UTTC. Fig. 9 documents a good accordance of measured and calculated results with deformations up to nearly 120 mm in mid-span. This corresponds to about l/30, so a rather pronounced value.

4. DESIGN CHART

The findings above are finally used to provide a practical design chart to allow for assessing load bearing capacities of SFRC cross-sections reinforced with rebar and subjected to UTTC for 90 minutes (R90). In addition to the well-known fundamentals of bending design of reinforced concrete structures in ultimate limit state (ULS) the following assumptions and restrictions have been made to derive the design chart in Fig. 10:

- Rectangular cross-section in pure bending (M_{Ed}, $N_{Ed} = 0$)
- Pre-defined relative geometrical position of rebar d_1/d
- Cross-section heated from one side for 90 minutes acc. to UTTC
- Heat transmission is independent from the steel fibre amount relevant to this purpose
- Temperature-dependent stress-strain relations of quarzitic aggregate concrete acc. to (DIN 2010 a)
- Temperature-dependent stress-strain relations of cold-formed rebar (class N) acc. to (DIN 2010 a)
- Temperature-dependent softening of stress-strain relation of SFRC acc. to Eq. (6) and (DBV 2001)
- Shape of stress-strain curve of post cracking tensile strength of SFRC modeled as a stress block acc. to (DAfStb 2015 b)
- Common strain levels in ULS ($-3.5 < \varepsilon_{c2} < 0$ and $0 < \varepsilon_{s1} < 25$ or rather $0 < \varepsilon^f_{c1} < 25$ [‰]) (DAfStb 2015 b)
- Design at normal temperatures acc. to (DAfStb 2015 b)
- Partial safety factor $\gamma_M = 1.0$ in case of fire acc. to (DIN 2010 a)

The assumption of constant strain limits in ULS in cases with and without fire exposure made here is conservative, because (DIN 2010 a) even defines enlarged strain boundaries with increasing temperature. The application of the design chart in Fig. 10 performs stepwise from the right to the left:

- Calculation of dimensionless moment μ_{Ed} at normal temperature
- Read mechanical reinforcement ratio ω from diagram. ω depends on the dimensionless post cracking tensile strength of SFRC α^f. Both parameters are related to normal temperatures.
- Shift to the left part of the design chart to get the point of intersection with the sets of curves obtained for the cross-section's height h and α^f.
- Read from diagram $\mu_{Ed,fire}$ denoting the residual dimensionless load bearing capacity in case of fire.
- Check for $\mu_{Ed,fire} / \mu_{Ed} > \eta_{fi}$ acc. to EC 2 to ensure a sufficient load bearing capacity in fire.

A calculation example for fire design (R90) of reinforced and steel fibre reinforced concrete by use of the design tool is given in (Heek et al. 2015).

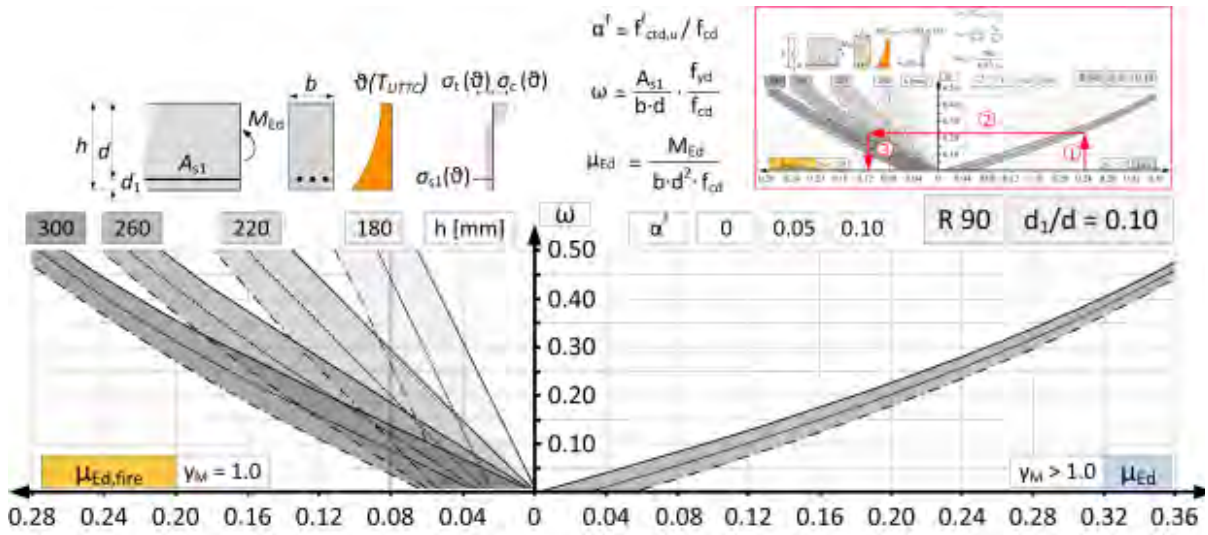

Fig. 10. Design chart to determine bearing capacities of rectangular steel fibre reinforced concrete cross-sections subjected to fire for 90 minutes (R90).

The design chart (Fig. 10) illustrates the decisive influence on the temperature-dependent load bearing capacity of the rebar's position (d_1) with respect to the outermost fibre of a cross-section subjected to fire. In case of a too small distance between rebar and the outer edge in fire, a sufficient residual bearing capacity η_{fi} cannot be established. Giving an approximation, EC 2 recommends a distance greater than 30 mm for reinforced concrete beams and one-way slabs subjected to one-sided elevated temperatures.

5. CONCLUSIONS

Test on six slabs made of reinforced concrete containing variable amounts of steel fibres subjected to both elevated temperatures due to UTTC and permanent mechanical loadings, lead to the following conclusions:

- Dosages of steel fibres up to approximately 1.0 vol. % do not significantly affect heat transmission in concrete cross-sections. For simplification, the derivation of temperature profiles can be done neglecting the effects of steel fibres.

- Steel fibres in reinforced concrete cross-sections provide benefits in terms of fire resistance, temperature-dependent load bearing capacities and load deformation behaviour.

- The temperature-dependent but strain-independent softening factor to determine the residual post cracking tensile strength of SFRC acc. to (DBV 2001) enables a recalculation of experimental data with high accuracy. The approach is appropriate to predict test results from literature in a reliable and realistic way on average.

- Fire design should consider temperature-dependent residual post cracking tensile strength of SFRC. Because of the large scatter reported in literature (e.g. (Kim et al. 2015)), further research is necessary to determine a sufficient partial safety factor γ_M in case of fire.

6. ACKNOWLEDGEMENTS

The financial support of the reported tests by the company NV Bekaert SA is gratefully acknowledged.

REFERENCES

[1] Balazs, G., Lubloy, E. (2012) “Reinforced Concrete Structures In And After Fire.” Concrete Structures, pages 72–80, Hungary.

[2] Caverzan, A. (2010) “High strain-rate uniaxial tensile constitutive behaviour in fibre reinforced cementitious composites.” PhD-thesis, Mailand, Italy.

[3] Chen, G.M., He, Y. H., Yang, H., Chen, J. F., Guo, Y. C. (2014) “Compressive behaviour of steel fibre reinforced recycled aggregate concrete after exposure to elevated temperatures.” Construction and Building Materials, 71, pages 1–15, Netherlands.

[4] Colombo, M. (2006) “FRC Bending Behaviour: A Damage Model for High Temperatures.” PhD-thesis, Mailand, Italy.

[5] Diederichs, U. (1999) “Hochtemperatur- und Brandverhalten von hochfestem Stahlfaserbeton.” Betonbau – Forschung, Entwicklung und Anwendung (ed. Teutsch, M.), Schriftenreihe des Instituts für Baustoffe, Massivbau und Brandschutz, H. 142, pages 67–76, Braunschweig, Germany.

[6] Falkner, H., Grunert, J.-P. (2011) “Faserbeton.” Betonkalender 2011: Kraftwerke, Faserbetonbau (eds. Bergmeister, K., Fingerloos, F., Wörner, J.-D.), Band 2, Ernst & Sohn, pages 1–19, Berlin, Germany.

[7] German Committee of Reinforced Concrete (DAfStb), (2015 a) “Commentary on the DAfStb Guideline ‘Steel Fibre Reinforced Concrete’” (DAfStb-Heft 614), Berlin, Germany.

[8] German Committee of Reinforced Concrete (DAfStb), (2015 b) “DAfStb Guideline ‘Steel Fibre Reinforced Concrete.’” DAfStb-Heft 614, Berlin, Germany.

[9] German Concrete and Construction Engineering Association (DBV), (2010) “DBV-Merkblatt Stahlfaserbeton.” Germany.

[10] German Fire Protection Association (vfdb), (2013) “Leitfaden Ingenieurmethoden des Brandschutzes.” Technischer Bericht vfdb TB 04-01 (ed. Hosser, D.), Braunschweig, Germany.

[11] German Institute for Standardization (DIN), (2010 a) “DIN EN 1992 (Eurocode 2) – Bemessung und Konstruktion von Stahlbeton- und Spannbetontragwerken – Teil 1-2: Allgemeine Regeln – Tragwerksbemessung für den Brandfall.” Beuth Verlag, Germany.

[12] German Institute for Standardization (DIN), (2010 b) “DIN EN 1993 (Eurocode 3) – Bemessung und Konstruktion von Stahlbauten – Teil 1-2: Allgemeine Regeln – Tragwerksbemessung für den Brandfall.” Beuth Verlag, 2010-12, Germany.

[13] German Institute for Standardization (DIN), (2012) “DIN EN 1363 – Feuerwiderstandsprüfungen – Teil 1: Allgemeine Anforderungen.” Beuth Verlag, Germany.

[14] Heek, P., Mark, P. (2014) “Non-linear analysis of SFRC elements bearing capacities accounting for tension stiffening by means of modified moment-curvature relations.” Proc. 1st ACI-fib Joint Int. Workshop on Fibre Reinforced Concrete, pages 292–309, Canada.

[15] Heek, P., Tkocz, J., Thiele, C., Vitt, G., Mark, P. (2015) “Fasern unter Feuer - Bemessungshilfen für stahlfaserverstärkte Stahlbetondeckenplatten im Brandfall.” Beton- und Stahlbetonbau 110 (10), pages 656–671, Germany.

[16] Hertel, C., Orgass, M., Dehn, F. (2002) “Brandverhalten von faserfreiem und faserverstärktem Beton.” Faserbeton – Innovationen im Bauwesen (eds. König, G., Holschemacher, K., Dehn, F.), Bauwerk Verlag, pages 63–76, Germany.

[17] Holschemacher, K., Weiße, D. (2004) “Bond of Reinforcement in Fibre Reinforced Concrete.” Proc. 6th RILEM Symp. Fibre Reinforced Concrete, BEFIB 2004 (eds. di Prisco et al.), pages 349–358, Varenna, Italy.

[18] Hosser, D., Richter, E., Kampmeier, B. (2013) “Konstruktiver Brandschutz nach den Eurocodes.” Betonkalender 2013: Lebensdauer und Instandsetzung, Brandschutz (eds. Bergmeister, K., Fingerloos, F., Wörner, J.-D.), Band 2, pages 1–62, Germany.

[19] Khaliq, W., Kodur, V. (2011) “Thermal and mechanical properties of fibre reinforced high performance self-consolidating concrete at elevated temperatures.” Cement and Concrete Research, 41, pages 1112–1122, Netherlands.

[20] Kim, J., Lee, G.-P., Moon, D. Y. (2015) “Evaluation of mechanical properties of steel-fibre-reinforced concrete exposed to high temperatures by double-punch test.” Construction and Building Materials, 79, pages 182–191, Netherlands.

[21] Mannsfeld, T. R. (2011) “Tragverhalten von Stahlbetonflächentragwerken unter Berücksichtigung der temperatur-bedingten Nichtlinearitäten im Brandfall.” PhD-thesis, Institut für Konstruktiven Ingenieurbau, Bergische Universität Wuppertal, Germany.

[22] Mark, P. (2003) “Optimierungsmethoden zur Biegebemessung von Stahlbetonquerschnitten.” Beton- und Stahlbetonbau 98 (9), pages 511–519, Germany.

[23] Tkocz, J., Heek, P., Mark, P., Thiele, C., Vitt, G. (2015) “SFRC slabs exposed to fire – experiments, temperature flow and design.” ALITinform International Analytical Review 41(6), pages 36–53, Russia.

[24] Zichner, T. (1976) “Temperaturunterschied infolge Witterungseinfluß und Beheizung von Massiven Brücken.” Forschung Straßenbau und Straßenverkehrstechnik, H. 212, Kirschbaum Verlag, Bonn-Bad Godesberg, Germany.